Formation and dissipation dynamics of the Asian Tropopause Aerosol Layer

Qianshan He
Shanghai Meteorological Service; Shanghai Key Laboratory of Meteorology and Health
Jianzhong Ma (majz@cma.gov.cn)
Chinese Academy of Meteorological Sciences
Xiangdong Zheng
Chinese Academy of Meteorological Sciences
Yanyu Wang
Fudan University
Yuhang Wang
Georgia Institute of Technology
Haizhen Mu
Shanghai Key Laboratory of Meteorology and Health
Tiantao Cheng
Fudan University
Ruilian He
Nanjing University of Information Science and Technology
Guan Huang
Donghua University
Dongwei Liu
Shanghai Key Laboratory of Meteorology and Health
Jos Lelieveld
Max Planck Institute for Chemistry

Research Article

Keywords: ATAL, ASM, QBO, CALIPSO, dynamics

Posted Date: August 19th, 2020

DOI: https://doi.org/10.21203/rs.3.rs-59990/v1

Abstract

The Asian Tropopause Aerosol Layer (ATAL) is characterized by enhanced aerosol concentrations in the Asian Summer Monsoon (ASM) anticyclone in the upper troposphere and lower stratosphere at 13-18 km altitude. A growing body of evidence suggests that the aerosol enhancement is closely connected with deep convection during the monsoon. However, the origin of the aerosols is under debate, and the key factors that determine the ATAL variability remain poorly understood. We investigated the formation and dissipation mechanisms of the ATAL and the inter-annual variation from a dynamical viewpoint using satellite observations and meteorological reanalysis data from 2012 to 2018. We identified the northern Bay of Bengal (BoB) and adjacent land area, where air pollution from the Indian subcontinent converges, as the major source area of aerosols to the ATAL. The spatial extent of the ATAL, represented by the mean Attenuated Scattering Ratio from satellite measurements, appears to be related to a secondary circulation driven by the stratospheric Quasi-Biennial Oscillation (QBO). The aerosols are not homogeneously distributed within the ATAL, and descending motion in the western part is found to play an important role in dissipation of the layer. These findings elucidate the ATAL dynamics and associated regional and global air pollution transports.

Significance Statement

The ATAL in the annually recurrent quasi-stationary anticyclone near the tropopause at 13- 18 km altitude is closely connected to deep convection during the ASM, and plays a key role in regional radiative forcing and climate change. We identified transport from the BoB and its surroundings as the major pathway of polluted air masses into the ATAL, based on satellite observations and meteorological data over the period 2012 to 2018. We also found that the ATAL variability is influenced by a secondary circulation related to the QBO in the stratosphere and descending motion in the western ATAL, the latter being a key factor in its dissipation. These findings explain the air pollution transport dynamics from the Indian subcontinent during the ASM.

Introduction

The Asian tropopause aerosol layer (ATAL) is characterized by enhanced aerosol extinction extending horizontally from the Eastern Mediterranean across India to Western China (~5–105°E; ~15-45°N) and vertically from about 13 km to 18 km altitude, and it forms in May/June with the onset of the Asian summer monsoon (ASM), while it dissipates around September with the breakup of the associated ASM anticyclonic circulation (1-3). Air pollution in the ATAL causes a significant regional radiative forcing, and is important for the aerosol loading of the global stratosphere, which significantly influences climate change (3, 4).

The ASM induces quasi-stationary anticyclonic circulation, located in the upper troposphere and lower stratosphere (UTLS) over Asia and the Middle East during boreal summer and flanked by the subtropical westerly jet to the north and the equatorial easterly jet to the south (5-11). The ASM occurs as a response to the diabatic heating associated with persistent deep convection, which results in rapid vertical transport of near-surface air from Southeast and South Asia and confinement of the air masses by the strong anticyclone during summer (12, 13). The mean upward circulation, especially at the eastern side of the anticyclone extends the transport into the lower stratosphere. The ASM offers a pathway for the transport of anthropogenic pollutants from the boundary layer into the UTLS through convective overshooting and into the stratospheric Brewer-Dobson Circulation (BDC) (6, 11, 14-17). Previous studies have concluded that deep convection can efficiently transport aerosols and their precursors from the boundary layer into the interior of the anticyclone, where they can be trapped for several months, subject to slow, large- scale ascent and weak lateral exchange with air masses outside the anticyclone (7, 18). However, if the polluted air would be fully confined in the interior of the anticyclone with continuous intrusions of fresh aerosols and gaseous precursors, the ATAL intensity would increase ceaselessly throughout the ASM period, from the onset until the breakup of the associated anticyclonic circulation. But in fact, the ATAL intensity remains approximately constant during the ASM period. Therefore, we expect mechanisms which play a role in maintaining the balance of the ATAL intensity throughout the ASM period.

Deep convection occurs in different areas within the ASM region, most frequently over the Bay of Bengal (BoB), North India, the South China Sea, the Southern Tibetan Plateau (TP), and the central TP (6, 19-22). A study by Chen et al. (23), based on Lagrangian model simulations driven by Global Forecast System (GFS) wind fields, suggested that the boundary layer to UTLS transport is predominant over the Western Pacific region and the South China Sea, followed by the BoB and the South Asian subcontinent and, to a lesser extent, the TP. A few studies argued that the main air source within the ASM anticyclone is from the Indian subcontinent (21, 24, 25). The TP is located at the core region of the ASM, thereby acting as a significant transport pathway for pollutants to enter the stratosphere (6, 21, 22, 26). The formation of the ATAL is complex, as it involves not only dynamics (and deep convection) but also chemical (e.g., for secondary aerosols) and deposition processes, depending on environmental conditions (e.g., temperature and relative humidity) and geographical regions in which important emission sources of pollutants are located (both for aerosols and their gaseous precursors). Therefore, trajectory analysis without considering aerosol sources and sinks may not fully capture the transport of surface sources into the ATAL.

Atmospheric chemistry general circulation models have been used to simulate the formation of the ATAL (5, 25-30). Although all models could predict the general contours of the ATAL (i.e., enhancement of aerosols at the tropopause within the ASM anticyclone), there is controversy among the model analyses about the chemical components that dominate the ATAL and what are the most important emission sources. Vernier et al. (3) reported that the aerosol optical depth (AOD) of the ATAL had increased by a factor of three from the late 1990s to the early 2000s, exerting a short-term direct regional radiative forcing (RF) of -0.1 W m-2 at the top of atmosphere over 18 years, comparable to the total RF due to

increased CO2 over the same period. Note that Vernier et al. (3) calculated the RF based on the assumption that the ATAL was composed of sulfate and organic aerosols, while recent balloon measurements showed that nitrate was an important component of the ATAL while sulfate was below the detection limit (31). It should be noted that increased SO2 emissions in India, as reported by recent studies (e.g., ref. 32), cannot fully explain the trend of the ATAL. In addition to increasing emission sources, inter-annual changes in dynamic features associated with the ASM may influence the ATAL intensity. To the best of our knowledge, this issue has not been addressed in previous studies, although it is very important for understanding the ATAL extent, trends and accurately estimating the RF.

The ASM is subject to strong dynamic variability, oscillations and eddy shedding (e.g., refs. 7, 33-38). Inter-annual, dynamical processes, such as the Quasi-Biennial Oscillation (QBO), can play a role in transporting trace gases and aerosols from the surface to the UTLS (39, 40). The QBO, known to modulate tropical convection (27, 41, 42), consists of a primary circulation by alternate easterly-westerly stratospheric winds descending from about 30 km to the tropopause with a period of about 26–27 months (43). Although the QBO is confined to the tropics, the oscillation can induce secondary circulations in the extra-tropics and affect the temperate latitudes through changes in planetary wave ducting. Previous research focused on the influence of the QBO on the transport of trace gases and aerosols from the surface to the UTLS in the tropics (e.g., refs. 41, 44, 45). No work has been reported to quantify the relation of the inter-annual QBO variability with the ATAL intensity in the ASM region. In this study we bridge the gap with the help of long-term records of the QBO together with atmospheric vertical motion from the most recent ERA5 reanalysis data and the Attenuated Scattering Ratio (ASR) from the Cloud-Aerosol Lidar and Infrared Pathfinder Satellite Observations (CALIPSO) stratospheric aerosol product for the ASM region. We also investigated the potential mechanisms that balance the ATAL intensity against vertical transport by deep convection during the ASM period.

Results And Discussion

Fig. 1 shows the distribution of mean ASR in the UTLS and associated meteorological variables at 100 hPa during the ASM period for the years 2012 to 2018. It shows the pronounced mean anticyclonic (high pressure) and water vapor center in the UTLS, with strong easterlies in the tropics and westerlies in the extra-tropics, in conjunction with a cold center over the southern TP. Significant deep convection occurs over the west coast of India, the Bay of Bengal (BoB), northeastern India, and occasionally over the southern TP. These are well-known climatological features associated with the Asian summer monsoon (46-50). Pronounced enhancement in ASR with a magnitude ranging from 1.05-1.22 is found over the southern anticyclone, spanning the Arabian Peninsula, the Himalayan-Gangetic Plain (HGP) and the China South Sea, with the highest ASR appearing over the northern BoB, East India and Bangladesh. The regions with the maximum ASR largely overlap with those of the minimum tropopause temperature and deep convection, with the former being located to the north of the latter, where pollutants from nearby emission sources are abundant and can be transported upward by deep convection associated with the ASM (51). The most noteworthy aspect of the ASR is the confined local maximum over the BoB.

Note that in most years, except for 2012 and 2018, the ASR and deep convection maxima show notable differences with respect to the horizontal locations. The pronounced ASR enhancement is located north of the deep convection region. There is a pattern of strong enhancement of ASR between 15-25°N and 80-100°E, just over the northern BoB and Bangladesh, located at the northwestern edge of the extensive areas of the strongest convection. Compared to southeastern Asia and central India, higher AODs are found around the northern BoB and adjacent coastal areas (Fig. S1), where strong convection occurs as well. Therefore, the locations of largest aerosol loading in the PBL and deep convection indicate that the major pathway for the transport of aerosols and precursors to the tropopause is located at the northern BoB and adjacent land areas. The deep convection over the BoB triggers low-level convergence of polluted air from the Indian subcontinent. It appears that the aerosols transported to the UTLS over the northern BoB and adjacent land areas originate from anthropogenic sources since carbon monoxide, which is generally considered as a pollution tracer, takes on a similar regional distribution pattern (Fig. S2).

As shown in Fig. 1, the enhancements of ASR in the UTLS during the ASM period show large inter-annual differences from 2012 to 2018, with the ASR varying from a minimum of 1.058 in 2013 to a maximum of 1.075 in 2012, averaged over the ATAL region (15-45°N; 5-105° E) defined by Vernier et al. (1, 3). Since pollution emissions are not expected to be highly variable, changes in the activity of deep convection are likely responsible for the inter-annual variability in the ASR during the ASM period. It should be noted that the geographical location and range of strong anticyclonic circulation varied from year to year (see Fig. 1). The inter-annual variations in the intensity of the ATAL compared to that of the ASM were investigated based on the relationship between the regionally-averaged ASR in the ATAL and the QBO index for different ASM periods (see Fig. 2). The inter-annual fluctuations in the ASR appear to be synchronized with inter-annual QBO index variations. Higher ASR corresponds to the eastward (negative) phase of the QBO and lower value matches westward (positive) phase. The highest ASR corresponds to the lowest QBO index in 2012, and vice versa in 2013. The ASR and QBO show an anti-phase relationship with a correlation coefficient of -0.78. The ASM intensity is affected by the QBO, and the correlation coefficient between the QBO index and the ASM intensity Index (ASMI) was calculated to be as high as 0.91 for the years 2012 to 2018 (see Fig. S3).

Previous work has shown that the QBO-induced secondary circulation is associated with an increase in upwelling during the easterly shear phase and a suppression of the upwelling during the westerly phase (52), and large anomalies of annual cycle variations in water vapor and other trace gases are due to the QBO disruption (44). The regionally averaged ASR in 2013, when the QBO index was in the westerly phase characterized by suppression of upwelling, is relatively lower than that in 2012, 2014 and 2018, when the negative QBO index was in the easterly shear phase. This result is consistent with the conclusion about the variation in water vapor during the 2015–16 QBO disruption by Tweedy et al. (53). We also investigated the relationship between the regionally averaged CO mixing ratio and the QBO index for different ASM periods, and the result also shows a correlation, although not as significant as that between the ASR and the QBO (Fig. 2). Atmospheric CO levels over South Asia are significantly influenced by biomass burning, and a close relationship between the CO mixing ratio in the UTLS region and the

carbon emission flux from biomass burning is found (R=0.79, Fig. S4). The increasing trends of ASR with CO mixing ratio underscore the influence of anthropogenic pollution on the formation of the ATAL. As mentioned above, we applied the latitude and longitude range of 15-45°N and 5-105°E to average the ASRs over the ATAL region. Sensitivity tests show that small differences in selected latitude and longitude range does not substantially change the inverse relationship between the ASR and the QBO (see Table S1).

The increase in tropopause ASR with decreasing QBO index can be attributed to dynamic processes, i.e., the intensification of the secondary circulation driven by the QBO. Fig. 2 also shows that deep convective activity increases with decreasing QBO index, being strongest between 10 and 20°N during the extreme easterly shear phase. Deep convective activity is gradually suppressed with an increasing QBO index. Collimore et al. (41) investigated the mechanisms linking the QBO with deep convection and found that the QBO modulation of tropopause height can allow convection to penetrate deeper. Therefore, deeper convection favors the transport of aerosols and gaseous precursors from the PBL to the tropopause.

We further explored the inter-annual variations of the three-dimensional structure of the vertical velocity with the QBO. The latitude-height cross-sections of the vertical velocities and the difference between 2012 and 2013 at the 90°E cross section are shown in Fig. S5. These two years, characterized by the extreme QBO index during the easterly and westerly phase, respectively, are particularly suitable to demonstrate the difference in vertical velocity induced by the QBO secondary circulation. Three outstanding columns with stronger upwelling motion, reaching the UTLS and capped near 100-90 hPa, are identified at about 18°N, 25°N and 32°N during the easterly phase in the year 2012. This QBO-associated secondary circulation anomaly produces upwelling by -0.05 Pa s−1 with a peak of -0.15 Pa s−1 at the southern flank of the TP, which facilitates the entry of tropospheric constituents into the subtropical lower stratosphere. The increased subtropical upwelling also supports the transport of aerosols from the upper troposphere to the lower stratosphere. As found in previous studies (e.g., refs. 27, 42), this instability develops in association with the QBO-derived secondary circulation near the UTLS. Interestingly, the descending motion over the region north of the TP is suppressed during the easterly phase of the QBO in 2012. This configuration of atmospheric vertical motion helps maintaining a balance of the ATAL intensity.

A most striking feature of the ATAL is the asymmetry in the regional distribution of enhanced aerosol levels even within the anticyclone. Relatively high ASR on the southeast of the anticyclone coincides with the strong convection between 40°E to 120°E and 10°N to 30°N. To the west of this strong convection region, there is a gradual decrease of ASR associated with downward transport and westward advection from the hot spot over the BoB, where the largest enhancement of ASR has been found (see Fig. 1). We analyzed this asymmetry distribution of ASR together with the vertical velocity from the ERA5 data, and noticed that the spatial distribution of enhanced aerosol in the UTLS was closely related to the horizontal cycle and vertical motion. During the ASM period, westerlies and descending motion prevail over the Middle East and northeastern Africa (Fig. 1). This overlap between the main descent region and the low ASR indicates that aerosol particles have been transported into the upper troposphere region below 12 km

altitude within the ASM anticyclone. This finding can explain the significant reduction of aerosols in the northern ASM region. Past studies showed that the aerosols transported into the lower stratosphere by the monsoon convection are confined within the strong anticyclonic circulation until breakup of the associated ASM anticyclone followed by recirculation in the lower stratosphere (12, 13, 27, 54). The asymmetry distribution of enhanced aerosols reveals a significant sink within the ASM region.

We selected a vertical cross section at 0-60°E and 90°E of the western anticyclone to demonstrate the role of downward transport in this area, which plays a key role in balancing the ATAL intensity. For quantitative comparison, we calculated the average extinction coefficients in the upper troposphere (6-12 km) and the vertical velocity at 100 hPa, and the ASR in the UTLS at the vertical cross section. As shown in Fig. 3b, there is a clear relationship between the vertical velocity and the upper tropospheric extinction coefficient. The load of UTLS aerosols in the western anticyclone can also impact the concentration levels further downward through descending motion in the upper troposphere, as indicated by the similar inter-annual variation trends between the extinction coefficient and ASR for the years 2015 to 2018. However, their relationship is not significant for the period before 2015. Statistical analysis indicates that the correlation of the extinction coefficient with ASR does not meet the 95% confidence level of student *t* test (see Table S2). A possible reason for this asynchronic variation is that the transport capacity of aerosols by descending motion approaches saturation for the abundant aerosol loading in the UTLS. But it is evident that the descending motion can play a role in the dissipation of the ATAL.

To summarize, Fig. 4 illustrates the horizontal movement of the aerosols within the anticyclone and the vertical transport pathways in the troposphere that balance the intensity of the ATAL during the ASM season. Deep convection over the BoB plays a dominant role in the vertical transport of aerosols from the polluted boundary layer to the UTLS within the anticyclone, where they are transported westward by the equatorial easterly jet. At approximately 70°E the aerosol particles and precursor gases are partially removed from the UTLS by the large scale descending motion, resulting in a concentration reduction in the western part of the ASM anticyclone. Our analysis indicates that in addition to the large-scale ascending circulation inside and eddy shedding at the margins of the anticyclone (8, 35, 39), downward transport in the western part of the ASM anticyclone provides an important dynamical aerosol sink in the UTLS, which maintains a balance in the intensity of the ATAL.

Materials And Methods

The CALIPSO satellite is a part of the A-train constellation, which was launched in April 2006 to a Sun Synchronous polar orbit with 98.2° inclination at an altitude of 705 km (55). The constellation repeats the cycle every 16 days with local equator crossing times of nearly 01:30 h and 13:30 h (55). The Cloud-Aerosol Lidar with Orthogonal Polarization (CALIOP) is one of the main instruments on board the CALIPSO satellite with a dual-wavelengths (532 nm and 1064 nm) polarization sensitive lidar. CALIOP provides profiles of clouds and aerosols and is capable of detecting clouds with an optical depth of 0.01 or less. We utilized level 3 global distribution of monthly gridded stratospheric aerosol profile data of 532 nm ASR (https://eosweb.larc.nasa.gov/project/calipso/cal_lid_l3_stratospheric_apro-standard_v1-00) to

investigate the distribution and intensity of ATAL from 2012 to 2018. This profile data is available on a monthly basis with 900 m vertical resolution from 8.2 km to 36.2 km and 20 ° longitude by 5° latitude horizontal resolution. The ASR averaged in the range of 13-18 km is used to represent the intensity of ATAL (see Fig. 1). We also utilized level 3 global distribution of monthly gridded tropospheric aerosol profile data of 532 nm extinction coefficient (https://eosweb.larc.nasa.gov/project/calipso/cal_lid_l3_tropospheric_apro_cloudfree-standard-V4-20) to investigate the transportation and linkage of tropospheric aerosol to the ATAL (see Fig. 3). The version 4.20 release of the CALIPSO lidar level 3 tropospheric aerosol profile product was released in September 2019. The new level 3 product is constructed from version 4 level 2 input data which are the highest quality and most sophisticated of all CALIOP level 2 data products. New level 3 quality screening procedures have been implemented to improve the quality of statistics reported by the product. This profile data has a 60 m vertical resolution from 0 km to 12 km and horizontal resolution of 2° latitude by 5° longitude.

The Level-3 MODIS Atmosphere Monthly Global Product MOD08_M3 (https://atmosphere-imager.gsfc.nasa.gov/products/) is used to investigate the AOD variation in the ASM region. The monthly dataset involves the AOD over both land and ocean with a horizontal resolution of 1° latitude by 1° longitude.

The most recent ERA5 reanalysis, which was released by the European Centre for Medium- Range Weather Forecasts (ECMWF) in 2018, has been used. Compared to ERA-Interim (56), the ERA5 data assimilation system uses the new version of the integrated forecasting system (IFS Cycle 41r2) instead of IFS Cycle 31r2 by ERA-Interim. In addition, various newly reprocessed data sets, recent instruments, cell pressure correction stratospheric sounding units (SSU), improved bias correction for radiosondes, etc., are renewed in ERA5. Shangguan et al. (57) evaluated the representation of temperature and ozone in the UTLS and concluded that ERA5 is significantly improved compared to ERA-Interim by better agreement with the Global Navigation Satellite System radio occultation (GNSS RO) temperature. The monthly meteorological fields contained in the ERA5 data are available on 60 hybrid model levels from the ground to 0.1 hPa at a spatial resolution of 2.5°×2.5°. The geopotential height, temperature, specific humidity and horizontal wind at the 100 hPa level as well as vertical velocity at 37 pressure levels from 1000 to 1 hPa are selected in this study. The ASM intensity Index (ASMI) is defined as follows (58),

ASMI = U100− U500

Where U is the regionally averaged monthly zonal wind at the corresponding barometric surface, indicated as subscript over the domain (40–110°E, 0–40°N). A higher ASMI refers to stronger vertical wind shear and enhanced monsoon circulation.

The OLR averaged over this region is an indicator of convective forcing; hence the OLR time series can be used as a proxy of monsoon convection (7). NOAA interpolated OLR at a spatial resolution of 2.5°×2.5° is used as a proxy for convection. This data was downloaded from https://www.esrl.noaa.gov/psd/data/gridd ed/data.interp_OLR.html.

For the QBO, we used the normalized monthly mean zonal winds (m s^{-1}) at 30 hPa level over Singapore (1°N, 104°E) as QBO index. This data set is available at http://www.geo.fu-berlin.de/met/ag/strat/produkte/qbo.

Topography information is provided at the Global Multi-resolution Terrain Elevation Data 2010 (GMTED2010) website (http://www.temis.nl/data/gmted2010/) of the U.S. Geological Survey (USGS) and the U.S. National Geospatial-Intelligence Agency (NGA).

Declarations

Acknowledgments

This study was supported jointly by the National Natural Science Foundation of China (Grant No. 91637101, 91837311 and 91537213).

Competing interests

The authors declare no competing interests.

References

1. Vernier, J. -P., Thomason, L. W. & Kar, J. CALIPSO detection of an Asian tropopause aerosol layer. Geophys. Res. Lett. 38, L07804, doi:10.1029/2010GL046614 (2011).

2. Thomason, L. W. & Vernier, J.-P. Improved SAGE II cloud/aerosol categorization and observations of the Asian tropopause aerosol layer: 1989–2005. Atmos. Chem. Phys. 13, 4605–4616 (2013).

3. Vernier, J. -P. et al. Increase in upper tropospheric and lower stratospheric aerosol levels and its potential connection with Asian pollution. J. Geophys. Res. Atmos. 120, 1608–1619 (2015).

4. Yu, P. et al. Efficient transport of tropospheric aerosol into the stratosphere via the Asian summer monsoon anticyclone. P. Natl. Acad. Sci. USA. 114, 6972–6977 (2017).

5. Li, Q. et al. Convective outflow of South Asian pollution: A global CTM simulation compared with EOS MLS observations. Geophys. Res. Lett. 32, L14826 (2005).

6. Fu, R. et al. Short circuit of water vapor and polluted air to the global stratosphere by convective transport over the Tibetan Plateau. P. Natl. Acad. Sci. USA. 103, 5664–5669 (2006).

7. Randel, W. J. & Park, M. Deep convective influence on the Asian summer monsoon anticyclone and associated tracer variability observed with Atmospheric Infrared Sounder (AIRS). J. Geophys. Res. Atmos. 111, D12314 (2006).

8. Park, M. et al. Transport above the Asian summer monsoon anticyclone inferred from Aura Microwave Limb Sounder tracers. J. Geophys. Res. Atmos. 112, D16309 (2007).

9. Park, M. et al. Chemical isolation in the Asian monsoon anticyclone observed in Atmospheric Chemistry Experiment (ACE-FTS) data. Atmos. Chem. Phys. 8, 757–764 (2008).

10. Park, M. et al. Transport pathways of carbon monoxide in the Asian summer monsoon diagnosed from Model of Ozone and Related Tracers (MOZART). J. Geophys. Res. Atmos. 114, D08303 (2009).

11. Randel, W. J. et al. Asian monsoon transport of pollution to the stratosphere. Science, 328, 611–613 (2010).

12. Hoskins, B. J. & Rodwell, M. J. A model of the Asian summer monsoon. Part I: The global scale. J. Atmos. Sci. 52, 1329–1340 (1995).

13. Highwood, E. J. & Hoskins, B. J. The tropical tropopause. Q. J. Roy. Meteor. Soc. 124, 1579–1604 (1998).

14. Gettelman, A. et al. Impact of monsoon circulations on the upper troposphere and lower stratosphere. J. Geophys. Res. Atmos. 109, D22101 (2004).

15. Fueglistaler, S. et al. Tropical tropopause layer. Rev. Geophys. 47, RG1004 (2009).

16. Bian, J., Yan, R. & Chen, H. Tropospheric pollutant transport to the stratosphere by Asian summer monsoon. Chin. J. Atmos. Sci. 35, 897-902 (2011).

17. Srivastava, A. K. et al. Aerosol characteristics in the UTLS region: A satellite-based study over North India. Atmos. Environ. 125, 222-230 (2016).

18. Dethof, A. et al. A mechanism for moistening the lower stratosphere involving the Asian summer monsoon. Q. J. R. Meteorol. Soc. 125, 1079-1106 (1999)

19. Tzella, A. & Legras, B. A Lagrangian view of convective sources for transport of air across the Tropical Tropopause Layer: distribution, times and the radiative influence of clouds. Atmos. Chem. Phys. 11, 12517–12534 (2011).

20. Bergman, J. W. et al. Seasonal differences of vertical-transport efficiency in the tropical tropopause layer: On the interplay between tropical deep convection, largescale vertical ascent, and horizontal circulations. J. Geophys. Res. 117, D05302 (2012).

21. Bergman, J. W. et al. Boundary layer sources for the Asian anticyclone: Regional contributions to a vertical conduit. J. Geophys. Res. 118, 2560-2575 (2013).

22. Wright, J. S. et al. The influence of summertime convection over Southeast Asia on water vapor in the tropical stratosphere. J. Geophys. Res. 116, D12302 (2011).

23. Chen, B. et al. Climatological perspectives of air transport from atmospheric boundary layer to tropopause layer over Asian monsoon regions during boreal summer inferred from Lagrangian approach. Atmos. Chem. Phys. 12, 5827- 5839 (2012).

24. Yan, R. C. & Bian, J. C. Tracing the boundary layer sources of carbon monoxide in the Asian summer monsoon anticyclone using WRF-Chem. Adv. Atmos. Sci. 32, 943-951 (2015).

25. Lelieveld, J. et al. The South Asian monsoon— pollution pump and purifier. Science. 1126/science.aar2501 (2018).

26. Gu, Y., Liao, H. & Bian, J. Summer time nitrate aerosol in the upper troposphere and lower stratosphere over the Tibetan Plateau and the South Asian summer monsoon region. Atmos. Chem. Phys. 16, 6641-6663 (2016).

27. Fadnavis, S. et al. Transport of aerosols in to the UTLS and their impact on the Asian monsoon region as seen in a global model simulation. Atmos. Chem. Phys. 13, 8771-8786 (2013).

28. Neely, R. R. et al. The contribution of anthropogenic SO2 emissions to the Asian tropopause aerosol layer. J. Geophys. Res. Atmos. 119, 1571–1579 (2014).

29. Yu, P. et al. Composition and physical properties of the Asian Tropopause Aerosol Layer and the North American Tropospheric Aerosol Layer. Geophys. Res. Lett. 42, 2540-2546 (2015).

30. Ma, J. et al. Modeling the aerosol chemical composition of the tropopause over the Tibetan Plateau during the asian summer monsoon. Atmos. Chem. Phys. 19, 11587-11612 (2019).

31. Vernier, J.-P. et al. BATAL: The Balloon Measurement Campaigns of the Asian Tropopause Aerosol Layer. B. Am. Meteorol. Soc. 99, 955-973 (2018).

32. Krotkov, N. A. et al. Aura OMI observations of regional SO2 and NO2 pollution changes from 2005 to 2015. Atmos. Chem. Phys. 16, 4605-4629 (2016).

33. Yan, R. C., Bian, J. C. & Fan, Q. J. The impact of the South Asia High Bimodality on the chemical composition of the upper troposphere and lower stratosphere. Atmos. Ocean. Sci. Lett. 4, 229-234 (2011).

34. Pokhrel, S. et al. ENSO, IOD and Indian Summer Monsoon in NCEP climate forecast system. Clim. Dynam. 39, 2143-2165 (2012).

35. Garny, H. & Randel, W. J. Dynamic variability of the Asian monsoon anticyclone observed in potential vorticity and correlations with tracer distributions. J. Geophys. Res. Atmos. 118, 13421-13433 (2013).

36. Vogel, B. et al. Fast transport from Southeast Asia boundary layer sources to Nothern Europe: rapid uplift in typhoons and eastward eddy shedding of the Asian monsoon anticyclone. Atmos. Chem.

Phys. 14, 12745-12762 (2014).

37. Nützel, M., Dameris, M. & Garny, H. Movements, drivers and bimodality of the South Asian High. Atmos. Chem. Phys. 16, 14755-14774 (2016).

38. Luo, J. et al. Space – time variability in UTLS chemical distribution in the Asian summer monsoon viewed by limb and nadir satellite sensors. Atmos. Chem. Phys. 18, 12511-12530 (2018).

39. Garny, H. & Randel, W. J. Transport pathways from the Asian monsoon anticyclone to the stratosphere. Atmos. Chem. Phys. 16, 2703-2718 (2016).

40. Pan, L. L. et al. Transport of chemical tracers from the boundary layer to stratosphere associated with the dynamics of the Asian summer monsoon. J. Geophys. Res. 121, 14159-14174 (2016).

41. Collimore, C. C. et al. On the relationship between the QBO and tropical deep convection. J. Climate. 16, 2552-2568 (2003).

42. Nie, J. & Sobel, A. H. Responses of tropical deep convection to the QBO: cloud-resolving simulations. J. Atmos. Sci. 72, 3625-3638 (2015).

43. Baldwin, M. P. et al. The quasi-biennial oscillation. Rev. Geophys. 39, 179-229 (2001).

44. Schoeberl, M. R. et al. QBO and annual cycle variations in tropical lower stratosphere trace gases from HALOE and Aura MLS observations. J. Geophys. Res. 113, D05301 (2008).

45. Ding, Q. & Fu, Q. A warming tropical central Pacific dries the lower stratosphere. Clim. Dynam. 50, 2813- 2827 (2018)

46. Lau, M. & Li, M. T. The monsoon of East Asia and its global associations-a survey. B. Am. Meteorol. Soc. 65, 114-125 (1984).

47. Krishnamurti, T. N. Summer monsoon experiment-a review. Mon. Weath. Rev. 113, 1590-1626 (1985).

48. Yanai, M., Li, C. & Song, Z. Seasonal heating of the Tibetan Plateau and its effects on the evolution of the Asian Summer Monsoon. J. Meteorol. Soc. Jap. 70, 319-351 (1992).

49. Webster, P. J. et al. Monsoons: Processes, predictability and the prospects for prediction. J. Geophys. Res. Oceans. 103, 14451-14510 (1998).

50. Wu, G. et al. The influence of mechanical and thermal forcing by the Tibetan Plateau on Asian climate. J. Hydrom. 8, 770-789 (2007).

51. Randel, W. J., Zhang, K. & Fu, R. What controls stratospheric water vapor in the NH summer monsoon regions? J. Geophys. Res. Atmos. 120, 7988–8001 (2015).

52. Plumb, R. A. & Bell, R. C. A model of the quasi-biennial oscillation on an equatorial beta-plane. Q. J. R. Meteorol. Soc. 108, 335-352 (1982).

53. Tweedy, O. V. et al. Response of trace gases to the disrupted 2015–2016 quasi-biennial oscillation. Atmos. Chem. Phys. 17, 6813–6823 (2017) .

54. Fadnavis, S. et al. Potential modulations of pre-monsoon aerosols during El Niño: impact on Indian summer monsoon. Clim. Dynam. 49, 2279-2290 (2017).

55. Winker, D. M. et al. Overview of the CALIPSO mission and CALIOP data processing algorithms. J. Atmos. Ocean. Tech. 26, 2310-2323 (2009).

56. Dee, D. P. et al. The ERA-Interim reanalysis: configuration and performance of the data assimilation system. Q J. Roy. Meteor. Soc. 137, 553-597 (2011).

57. Shangguan, M., Wang, W. & Jin, S. Variability of temperature and ozone in the upper troposphere and lower stratosphere from multi-satellite observations and reanalysis data. Atmos. Chem. Phys. 19, 6659-6679 (2019).

58. Webster, P. J. & Yang, S. Monsoon and ENSO: selectively interactive systems. Quart. J. Roy. Meteor. Soc. 118, 877-926 (1992).

Figures

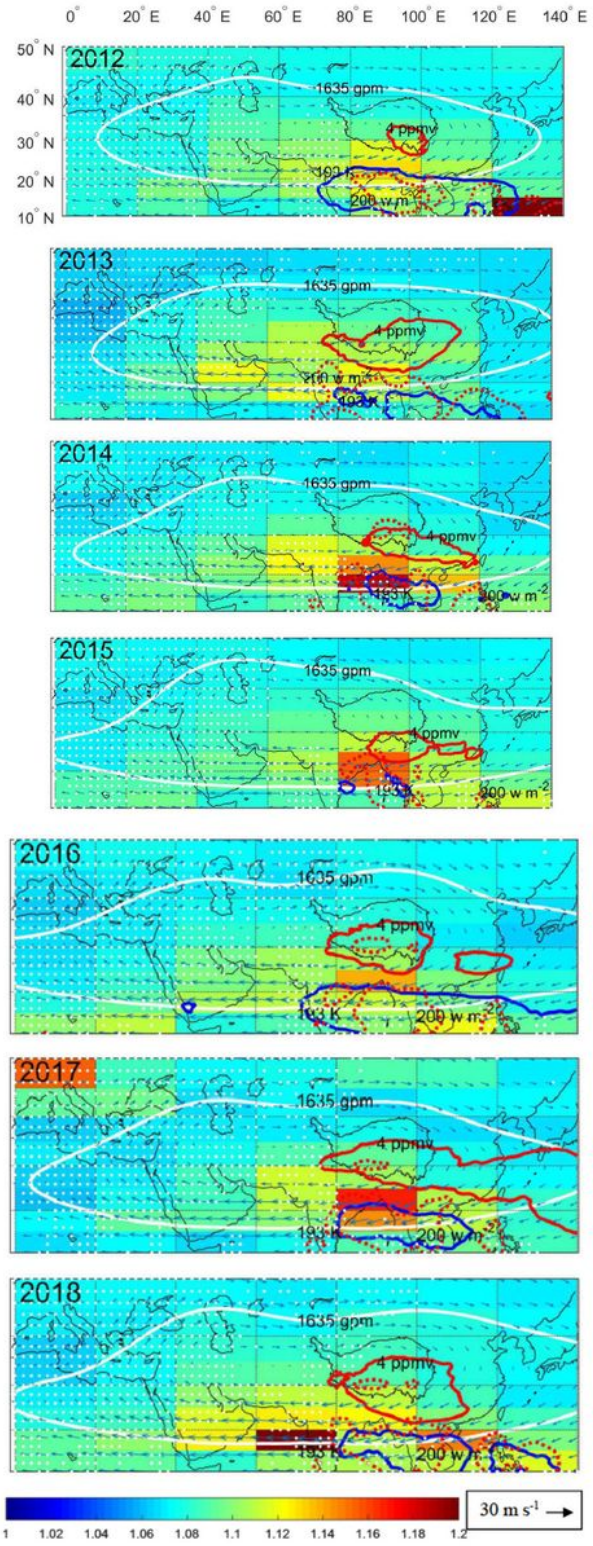

Figure 1

The distribution of mean ASR in the UTLS (at an altitude range of 13–18 km) over the ASM period for each year from 2012 to 2018 (color shading), superimposed with wind vectors and the contours of geopotential height at 1635 gpm (white solid line), temperature at 194 K (blue solid line), water vapor at 4 ppmv (red solid line) and Outgoing Long-wave Radiation (OLR) at 200 w m-2 (dashed contours) at 100 hPa. Locations with vertical motion speed > 0 Pa s-1 (indicating descent) are highlighted with white dots.

The coastline and outline of the TP are also indicated with black thin solid lines. A reference wind vector (30 m s-1) is shown in bottom right corner.

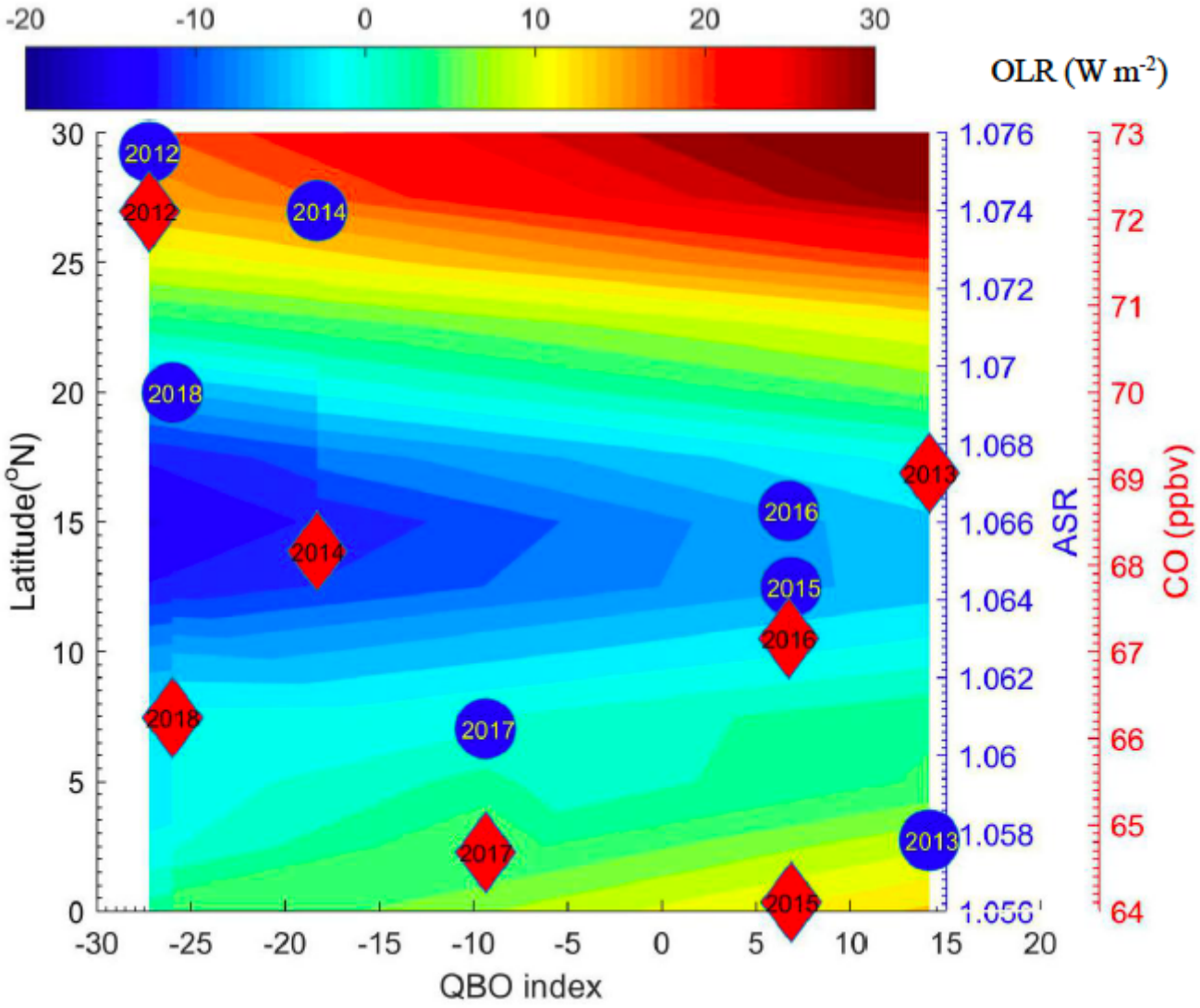

Figure 2

The relationship between the QBO index and the averaged ASR enhancement in the ATAL (blue cycles), as well as the average CO mixing ratio at 100 hPa in the ASM region (15- 45°N and 5-105°E), and the variation of zonal mean anomalous OLR (W m-2) in the convective regions (60 to 120°E) at different latitudes with the QBO index during the ASM period, for the 7 years from 2012 to 2018.

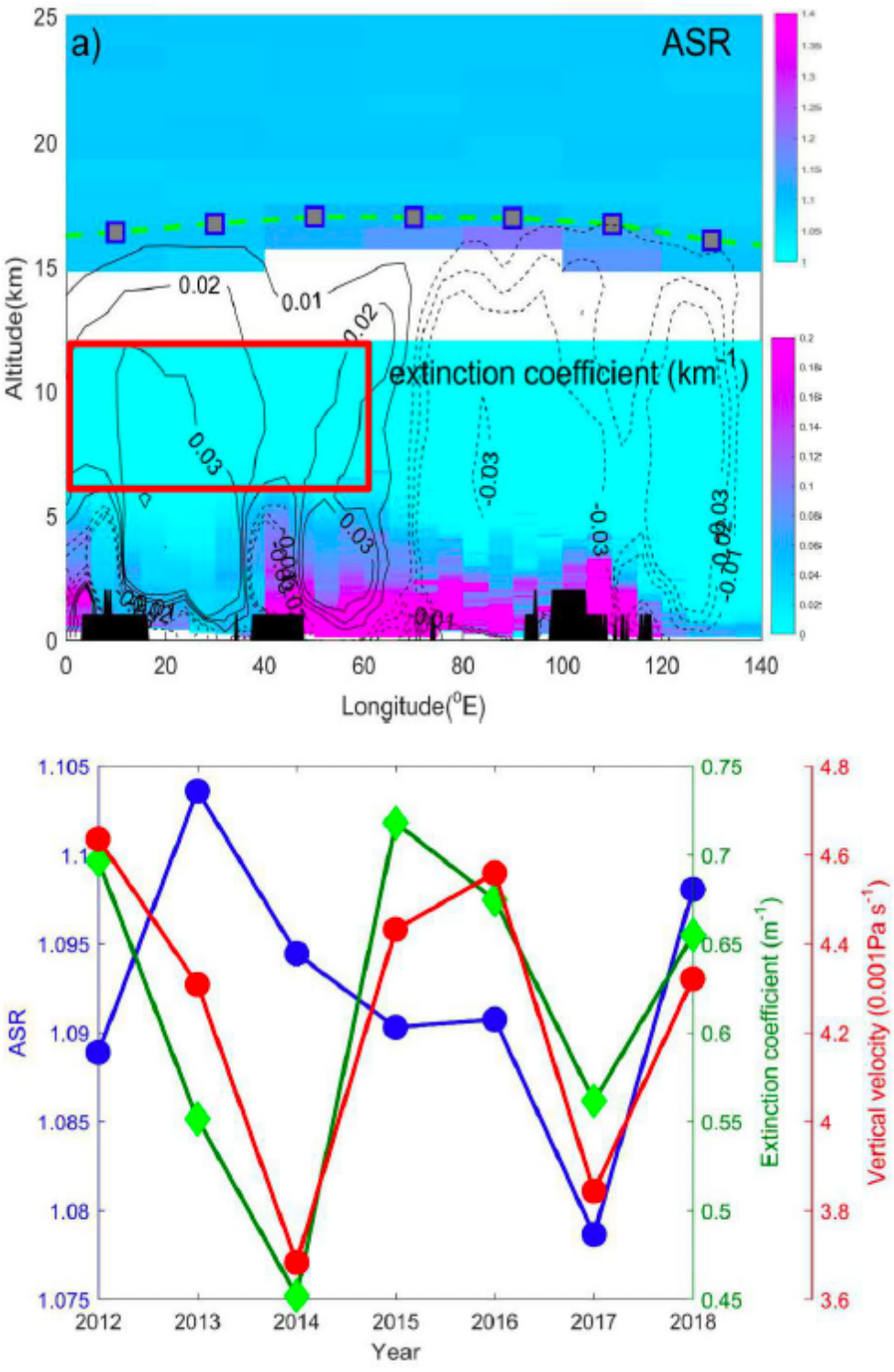

Figure 3

(a) Longitude-altitude cross section (0°-140°E) of the ASR and extinction coefficient over 24 the equatorial easterly jet (25°N) and associated vertical motion (Pa s-1) field with solid (dashed) 25 contours indicating descent (ascent), averaged over the ASM period in 2012. The squares with 26 green dashed line denotes the tropopause altitude derived from the CALIPSO satellite level 3 27 monthly stratospheric aerosol data during the same period. The black areas denote the terrain 28 height (km) above sea level. The red

rectangle denotes the upper troposphere below the western 29 ATAL domain (0-60°E). (b) The inter-annual variations of the average extinction coefficient in 30 the upper troposphere (6-12 km), the ASR in the UTLS (13-18 km), and the vertical velocity at 31 100 hPa for the western ATAL domain (0-60°E, 25°N).

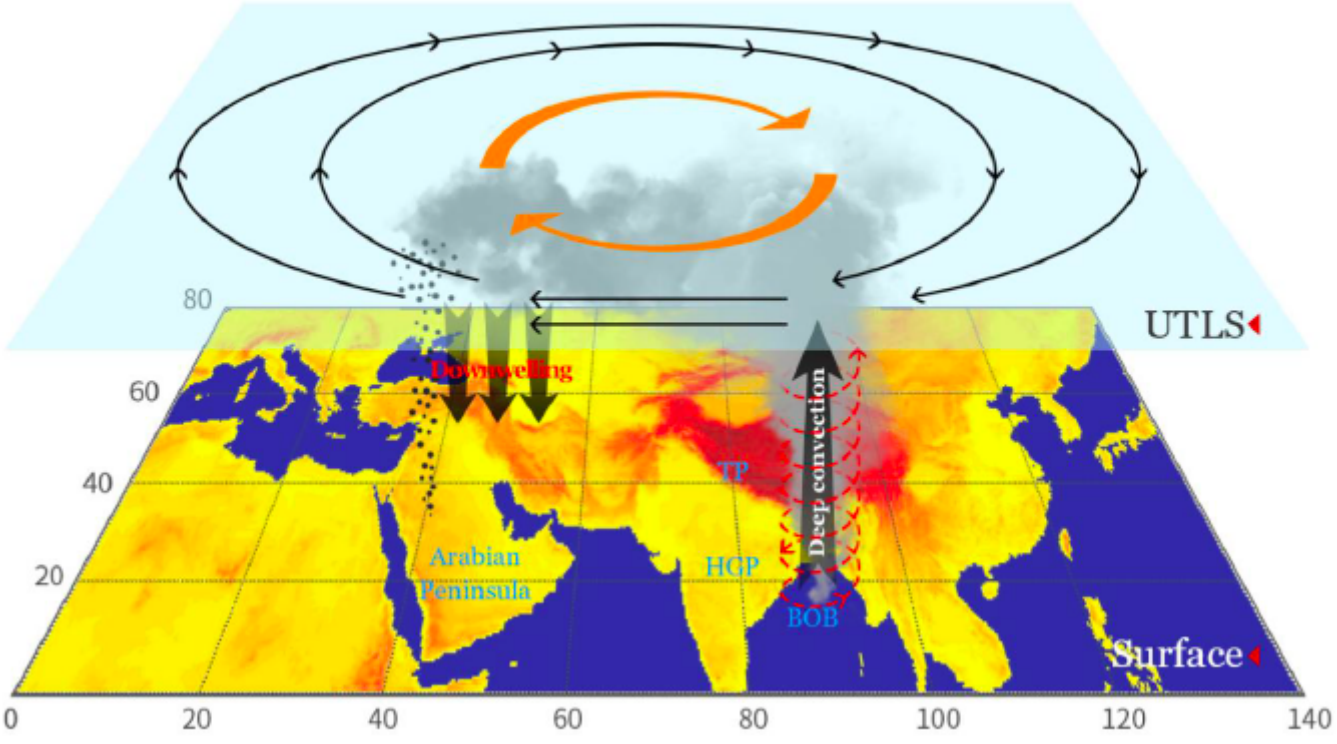

Figure 4

Schematic of the transport processes that indicate the formation and dissipation dynamics of the ATAL during the ASM.

Supplementary Files

This is a list of supplementary files associated with this preprint. Click to download.

- SupplementalMaterial.pdf